How to cite: *Angew. Chem. Int. Ed.* **2023**, *62*, e202308181
doi.org/10.1002/anie.202308181

VIP **Electroanalytical Chemistry** *Very Important Paper*

A Rapidly Responsive Sensor for Wireless Detection of Early and Mature Microbial Biofilms

Atefeh Shafaat, Juan Francisco Gonzalez-Martinez, Wanderson O. Silva, Andreas Lesch, Bhawna Nagar, Zita Lopes da Silva, Jessica Neilands, Javier Sotres, Sebastian Björklund, Hubert Girault, and Tautgirdas Ruzgas**

Abstract: Biofilm-associated infections, which are able to resist antibiotics, pose a significant challenge in clinical treatments. Such infections have been linked to various medical conditions, including chronic wounds and implant-associated infections, making them a major public-health concern. Early-detection of biofilm formation offers significant advantages in mitigating adverse effects caused by biofilms. In this work, we aim to explore the feasibility of employing a novel wireless sensor for tracking both early-stage and matured-biofilms formed by the medically relevant bacteria *Staphylococcus aureus* and *Pseudomonas aeruginosa.* The sensor utilizes electrochemical reduction of an AgCl layer bridging two silver legs made by inkjet-printing, forming a part of near-field-communication tag antenna. The antenna is interfaced with a carbon cloth designed to promote the growth of microorganisms, thereby serving as an electron source for reduction of the resistive AgCl into a highly-conductive Ag bridge. The AgCl–Ag transformation significantly alters the impedance of the antenna, facilitating wireless identification of an endpoint caused by microbial growth. To the best of our knowledge, this study for the first time presents the evidence showcasing that electrons released through the actions of bacteria can be harnessed to convert AgCl to Ag, thus enabling the wireless, battery-less, and chip-less early-detection of biofilm formation.

Introduction

Biofilms are defined as surface-attached microbial communities fixed in a matrix composed of extracellular polymeric substances, EPS, i.e., polysaccharides, proteins, DNA, and lipids. Biofilms can have lasting harmful effects especially when it comes to biofilm-triggered infectious diseases. Biofilms in general are impenetrable to antibiotics and antimicrobial agents and the biofilm formed on wound scabs, indwelling catheters, and hip and knee implants may thus perpetuate serious illnesses.[1] Among these, chronic wounds are experienced by almost 2 percent of the total population in any developed country, impacting not only the quality of life but also putting a financial burden on the individual and the society as a whole.[2] Consequently, assessment of biofilm formation using efficient diagnostic tools is vital in order to avoid virulent infections.[3] Standard clinical techniques for assessment of infections based on microbiological and molecular assays are performed routinely but they are time-consuming, and they require the patient to attend the clinic. Imaging assays are the most reliable evaluation techniques to verify biofilm formation but the need for appropriate instruments and trained operators makes them unsuitable in routine clinical settings.[4]

On-site assessment of biofilm growth relying on sensor technology and Internet of Things (IoT) has a strong potential to transform clinical-centered care to patient-centered care and attenuate the disease burden.[5] Recent

[*] A. Shafaat, J. Sotres, S. Björklund, T. Ruzgas
Department of Biomedical Science, Faculty of Health and Society, Malmö University
20506 Malmö (Sweden)
and
Biofilms - Research Center for Biointerfaces, Malmö University
20506 Malmö (Sweden)
E-mail: atefeh.shafaat@mau.se
tautgirdas.ruzgas@mau.se

J. F. Gonzalez-Martinez
Department of Applied Physics, Universidad Politécnica de Cartagena
30202 Cartagena (Spain)

W. O. Silva
Institute of Systems Engineering, HES-SO Valais-Wallis
1950 Sion (Switzerland)

A. Lesch
Department of Industrial Chemistry "Toso Montanari", University of Bologna
Viale del Risorgimento 4, 40136 Bologna (Italy)

B. Nagar, H. Girault
Laboratory of Physical and Analytical Electrochemistry, École Polytechnique Fédérale de Lausanne (EPFL) Valais Wallis
1950 Sion (Switzerland)

Z. Lopes da Silva, J. Neilands
Department of Oral Biology, Faculty of Odontology, Malmö University
20506 Malmö (Sweden)

advances regarding the tracking of microbial biofilms have introduced three classes of sensors, enabling the study of (*i*) whole bacteria embedded in EPS, (*ii*) the pH and temperature of the bacterial environs,[6] and (*iii*) the level of released matrix enzymes as potential biomarkers.[7] Combining the first approach with the concept of microbial fuel cells provides simple and efficient tools for tracking planktonic and biofilm bacteria. The technique relies on electrochemically active bacteria that convert chemical energy into electrical energy (i.e., the release or consumption of electrons) and monitoring the overall redox reaction, which can be then related to biofilm growth.[8]

Realizing the potential benefits of microbial fuel cells which require minimal construction and have straightforward data reading and processing characteristics, the researcher's attention turned towards wireless communication techniques with the aim of on-site, continuous, and remote sensing of biofilm formation.[9] However, the successful adaptation of wireless technology for tracking biofilm formation demands simple, cost-effective, and non-invasive devices. In this regard, systems functioning in chip-less and passive radio frequency identification (RFID) modes outperform integrated circuit (IC) based and active RFID transponders. A chip-based approach entails employing a dedicated silicon IC specifically designed to perform the sensing function. Chip-less sensing systems departure from traditional integrated circuits for operation. Instead, they harness electrical components to capture and transmit electrical signals, which are subsequently processed and analyzed by an external system.[10]

The cost of the IC-based RFID transponders, the need for chip programming, being confined to standardized sizes/forms of electronic chips and the difficulties in establishing a connection between chip and antenna in challenging physicochemical conditions directed our work toward designing a chip-less wireless sensing system that has the advantages of low-cost, flexibility and simple information encoding. We exemplified the importance of such wireless systems in our previous studies by interfacing biological oxidation or reduction reactions with an RFID tag antenna. The concept has been applied for wireless detection of hydrogen peroxide[11] and glucose[12] where enzymatic reactions based on horseradish peroxidase (HRP) or glucose dehydrogenase (GDH) oxidize silver nanoparticles (AgNPs) or reduce silver chloride (AgCl) as a part of tag antenna in the presence of the analyte. These studies, for the first time, illustrated the application of the Ag/AgCl redox conversion in simple, chip-less, and battery-less wireless sensing of enzyme-catalyzed reactions. However, the long response time and the irreproducibility of manual drop-casting of low amounts of silver nanoparticles limited these sensors from being practically competitive. Inkjet printing, a mask-free microfabrication technique, allows for precise and reproducible deposition of highly controlled masses of various nanomaterials on both rigid and flexible substrates. Besides an enormous flexibility in pattern design (e.g., electrode dimensions) and realization, the thickness and loading of nanoparticles on a substrate is highly controllable by the ink compositions and printing, as well as, by post-printing parameters. The technique is useful for prototyping and large-scale production, reaching simply by scaling industry production levels.[13]

Using the advantages of inkjet printing, we propose a wireless, and battery-less sensor based on chip-less RFID for fast detection of planktonic and biofilm bacteria. We showcase the potential of this simple and flexible sensor by investigating bacterial co-culture of *Staphylococcus aureus* (*S. aureus*) and *Pseudomonas aeruginosa* (*P. aeruginosa*), the most prevalent microorganisms isolated in chronic wound infections.[14] Scheme 1 shows the design of the sensor, which is an electrochemical cell comprised of two parts, i.e., the anode and the cathode. The anode is a carbon cloth with high conductivity for hosting the growth of microorganisms. The cathode is an AgCl layer prepared by electrochemical oxidation of an inkjet printed Ag, that bridges two insulated silver legs. In the presence of microorganisms, the growth of an electroactive biofilm on the carbon cloth anode provides electrons for conversion of the AgCl layer of the cathode into a conductive Ag bridge. The AgCl layer is a part of the passive tag antenna and any changes in its resistance can be detected wirelessly by the reader. Compared to our previous studies, the picolitre volumes of nanomaterials deposited by inkjet printing in the cathode layer enable shorter times of AgCl reduction by the microorganism populated anode. As a consequence, this leads to reproducibly rapid detection of microbial biofilm. Tracking biofilm formation using the proposed wireless sensor was performed in both standard growth medium and simulated wound fluid. The study provides fundamental results required for testing the applicability of this sensor in the form of a smart bandage enabling the detection of bacterial growth in a wound environment. Generalizing, based on a chip-less, wireless setup the findings in this work may provide the possibility of early detection of wound infection.

Results and Discussion

Scheme 1 shows the working principle of the wireless and battery-less biosensor which interfaces the growth of microbial biofilm on a carbon cloth (bioanode segment) to the Ag/AgCl redox conversion (cathode layer). The co-culture of *S. aureus* and *P. aeruginosa* has been selected to model chronic wound conditions with its most common isolated electroactive microorganisms. Upon contacting the carbon cloth, the planktonic bacteria attach to the surface in two successive steps, an initial reversible step followed by permanent attachment.[15] Further proliferation along with the secretion of EPS and maturation of the developed biofilm will occur in the next stages. In all of these steps, planktonic and biofilm bacteria communicate with the surface based on a mechanism called extracellular electron transfer (EET). The EET enables transfer of electrons from the bacteria to the surface which hosts their growth. In case of *P. aeruginosa*, it has been verified that at the anode, the species produce phenazine compounds such as phenazine-1-carboxylic acid, phenazine-1-carboxamide and pyocyanin

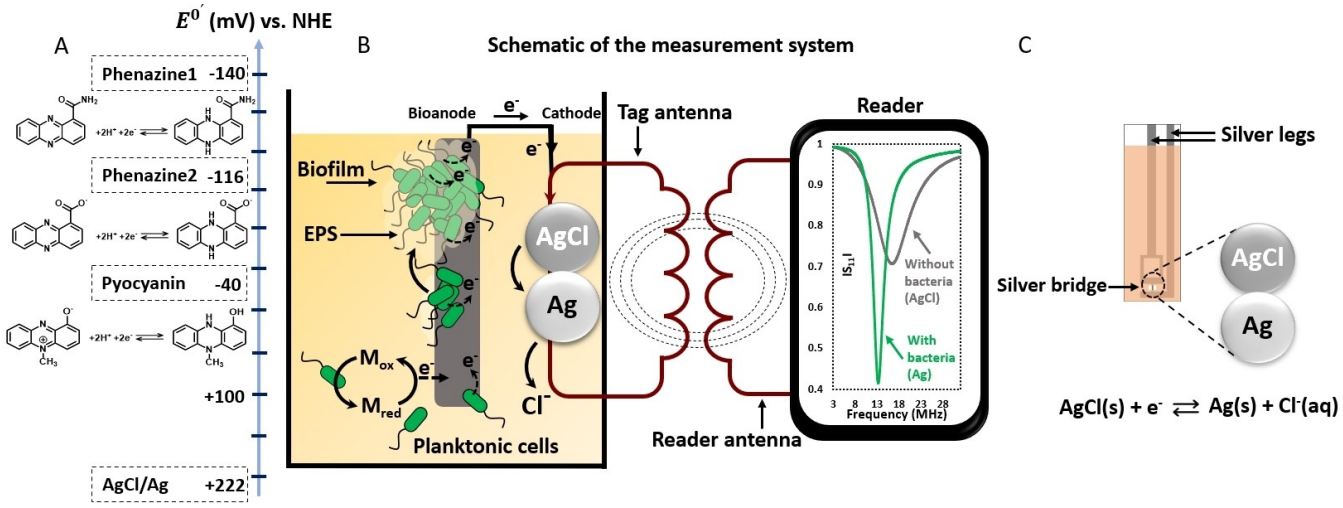

Scheme 1. **(A)** Structure and formal potential of the possible redox mediators secreted by *P. aeruginosa* at pH 7 in comparison with the redox potential of Ag/AgCl. Phenazine1 represents phenazine-1-carboxamide and Phenazine2 represents phenazine-1-carboxylic acid. **(B)** Schematic representation of the biosensor-RFID tag for the detection of planktonic or biofilm bacteria. The setup is comprised of two parts, i.e., the anode and the cathode. The carbon cloth anode serves as an external electrode for hosting the growth of microorganisms. The cathode in connection to the carbon cloth is an AgCl layer bridging two silver legs of the IJPE as shown in (C). The IJPE will be then located as a part of the tag antenna with a 5 mm removed antenna line for connection of two legs of IJPE bridged by AgCl. In the presence of the microorganisms, the growth of an electroactive biofilm on the carbon cloth will provide electrons for the conversion of the AgCl layer to conductive Ag. The AgCl layer is a part of the passive tag antenna and any changes in its resistance can be detected wirelessly by the reader due to the magnetic coupling between the reader antenna and the tag antenna. **(C)** The IJPE with two silver legs bridged by the AgCl layer which serves as the actual cathode, where the Ag/AgCl redox conversion takes place. To simplify the scheme, only the bridge is shown in (B). In the experimental setup (see SI), the AgCl/IJPE is integrated/coupled as a part of the tag antenna and connected to the carbon cloth anode as shown in (B).

which facilitate the electron transfer between cells and the electrode acting thus as mediators.[16] Considering the redox potential of these mediators shown in Scheme 1, it is expected that their electron transfer reactions at the anode drive the reduction of AgCl in the cathode layer.

Connecting to what is explained above, in this work, we aim to explore the feasibility of the wireless detection of planktonic and in particular biofilm bacteria. In brief, the hypothesis is that the electrons released from bacterial cells at the bioanode will be supplied to the cathode part of the tag antenna and reduce the non-conductive AgCl to highly conductive Ag. This transition strongly alters the impedance of the tag antenna which can be tracked wirelessly by measuring the antenna reflection coefficient, $|S_{11}|$, and characteristic frequency, f_0 of the biosensor-tag system. The hypothesis has been tested by the experiments described in the following paragraphs. These include observations of the bacterial attachment and biofilm development on carbon cloth using scanning electron microscopy and confocal laser scanning microscopy, measurements of the open circuit potential and the current developed by the growth of biofilm, optimization of the inkjet printed electrode (IJPE) characteristics for shortening the sensor response time and proof-of-concept demonstration of wired and wireless detection of biofilm in both standard growth medium and simulated wound fluid. The discussions will be then finalized with a presentation of the equivalent circuit of the biosensor tag to better understand the proposed wireless setup features.

Observation of bacterial attachment to carbon cloth by scanning electron microscopy (SEM) and confocal laser scanning microscopy (CLSM)

To observe bacterial attachment to the surface during the biofilm formation, SEM and CLSM experiments were conducted. For SEM imaging, the biofilm formed by the co-culture of the *S. aureus* and *P. aeruginosa* on carbon cloth was fixed from the early stages till the maturation levels. The results of these studies are important to examine the biofilm in terms of bacterial morphology and the timeframe during which initial attachment, proliferation and maturation occur. Figure 1A shows representative SEM images recorded after fixing bacteria at different time points from 30 min to 24 h. The 30 min results show the coexistence of two species of spherically-shaped *S. aureus* and rod-shaped *P. aeruginosa* attached to the carbon cloth fibers. After 2–4 h bacterial proliferation, their attachment as multilayer is visible. After 6–8 h proliferation, the secretion of the EPS is noticeable with obvious matrix formation, embedding the bacteria after about 10 h. The biofilm will then mature in the following stages (above 12 h), which is observable as higher number of surface attached microbial aggregates and larger area coverage.

The external electrode selected in this work for hosting the growth of microorganisms is a woven carbon cloth made by weaving the carbon fibers. The void space between fibers increases the area accessible for bacterial attachment. Comparing to SEM which gives an overall picture of the sample surface, CLSM enables to visualize bacterial cells at

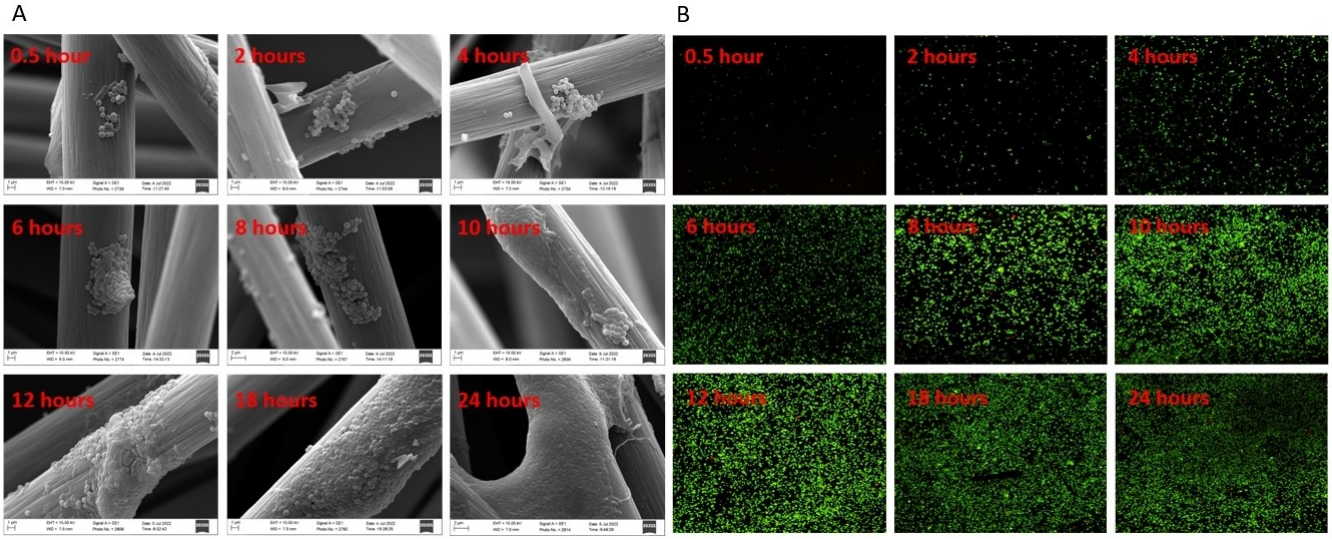

Figure 1. (A) SEM images obtained by fixing bacteria during biofilm formation on carbon cloth from the co-culture of *S. aureus* and *P. aeruginosa* (initial bacteria ration 10:1). (B) Growth steps of the biofilm formed by the co-culture of *S. aureus* and *P. aeruginosa* (10:1) visualized by CLSM after staining with the Live/Dead BacLight kit.

different depths of the biofilms. Figure 1B shows CLSM images at different time points from 30 min to 24 h. Increased microbial density and surface coverage are observable during the biofilm formation. The CLSM images correlate with the SEM images in all phases of the biofilm growth. Conducting SEM and CLSM imaging is valuable in determining the time points at which bacteria form aggregates or communities. It is reasonable to expect that a greater total number of bacteria attached to the electrode surface will be able to supply more electrons to the cathode, thus shortening the response time of the wireless device described later in the text.

Open circuit potential (OCP) and current measurements for monitoring the growth of biofilm on carbon cloth bioanode

Open circuit potential (OCP) measurements, a widely used technique when working with microbial fuel cells, was exploited in this work for tracking the development of a *S. aureus* and *P. aeruginosa* biofilm on carbon cloth. For this purpose, the carbon cloth was coupled to a double junction Ag/AgCl (3 M KCl (gel-based)) reference electrode and the changes in potential were recorded continuously for 24 h during the biofilm formation. As a negative control, measurements were conducted in bacteria-free LB medium (Figure S3). Figure 2A shows the OCP measurement over 24 h for three independent experiments in which the OCP changed from positive ($27\,mV \pm 1.2$) to negative values ($-163\,mV \pm 15$) during the first 7 hours. This is interpreted as a result of bacteria attachment and proliferation on the conducting cloth. At the 7 h timepoint, a sharp potential decrease was observed, corresponding to exponential bacterial growth. This step continues until 10 h and generates an OCP of $-262\,mV \pm 9.5$. Reaching a plateau at time points above 10 h is in accordance with the last stages of microbial growth where a matured biofilm has been formed on the surface. The negative potential developed on carbon cloth during the growth of a microbial biofilm could mainly result from the bacterial ability to transfer electrons to the surface by extracellular electron transfer.

To examine the EET, the current generated by the *S. aureus* and *P. aeruginosa* co-culture as well as the individual monocultures was measured in a three-electrode system comprising a carbon cloth working electrode. Figure 2B shows the current generated over 24 h. The current-time dependence reflects the EET at different stages of biofilm formation or bacterial growth including the lag phase, the log phase, and the stationary phase. Following a slight initial current increase, a sharp increase in current is observed at the 7 h time point. These significant alterations in current coincide with the considerable changes of potential (Figure 2C) signals that the biofilm bacteria transformed to a strongly electrogenic phenotype. As stated above, *P. aeruginosa* transfers electrons to the surface by secreting phenazine redox mediators. The produced phenazine derivatives by *P. aeruginosa* can be also exploited as the redox mediator (or electron shuttle) by *S. aureus* and they co-actively increase the density of the charge transferred to the electrode. The burst of current will however be delayed for 7 hours due to the presence of the less abundant *P. aeruginosa* in the co-culture as well as diffusion of the electron shuttles into the surroundings at the early stages. According to the results presented in Figure 2B, the current (or the equivalent charge shown in three regions with different colors) increases as the biofilm develops from the initial attachments (0.05 coulombs) to the maturation levels (2.73 coulombs); the importance of the generated charge to shorten the response time of the wireless biofilm sensor will be discussed later in the text.

Measurements of the current generated by the bacteria were also performed in individual monocultures of *S. aureus*

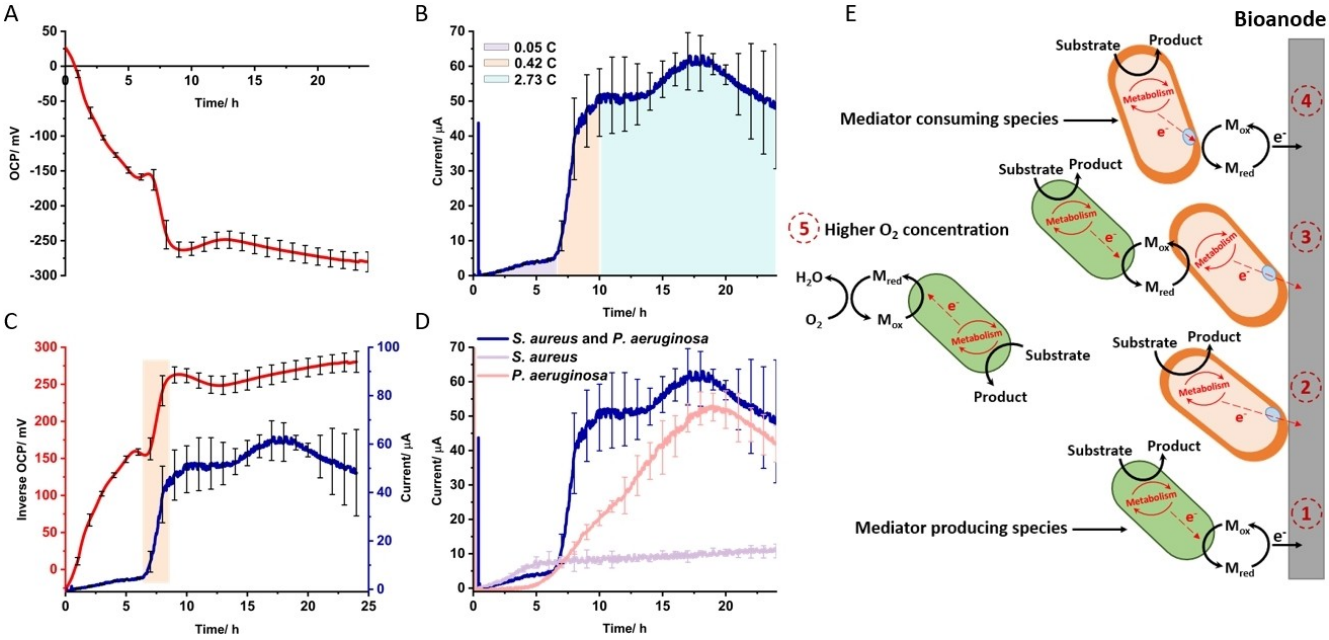

Figure 2. Measurement of (A) Open circuit potential (OCP) and (B) current developed on the carbon cloth during the formation of a biofilm from the co-culture of *S. aureus* and *P. aeruginosa;* initial bacterial concentration is 10^6:10^5 CFU/mL (10:1), respectively. The areas under the curve in (B), shown by different colors, represents the equivalent charge (in coulombs) calculated for different stages of biofilm formation. (C) Merge of the results of OCP (A) with amperometry (B) measurements shows the relation between these two measurements; the sign of OCP values has been inverted. (D) The current generated by carbon cloth electrode in monocultures of *S. aureus* (10^6 CFU/mL; initial bacteria concentration) or *P. aeruginosa* (10^5 CFU/mL) and their co-culture (10^6:10^5 CFU/mL). The error bars represent the standard deviation of measured data for three independent experiments. (E) Possible extracellular electron transfer pathways resulting in electrode current from planktonic and biofilm bacteria, which can synergistically share EET mediators; mechanisms 1–5 are explained in the text.

and *P. aeruginosa* (Figure 2D). Due to the higher concentration of *S. aureus* (10^6 CFU/mL) compared to *P. aeruginosa* (10^5 CFU/mL), more current was generated by *S. aureus* in the first hours (up to 7 h). However, being Gram-positive bacteria with thick non-conductive cell walls, only weak extracellular electron transfer is sustained, as confirmed in Figure 2D. On the other hand, *P. aeruginosa* exploits its secreted phenazine compounds as the electron shuttle and generates high current levels, mainly after 7 h. Comparing the currents generated by individual bacteria to the current provided by the co-culture, it can be concluded that these two species synergistically enhance the current delivered by bioanode.

Figure 2E, visualizes the explanations for the current generation by biofilm comprised of two types of mediator producing and mediator consuming (mediator-exploiting) species.[16e] Mechanism 1 refers to mediator producing *P. aeruginosa* which uses self-secreted phenazines as electron shuttle at the electrode surface as well as in the middle and top layers of biofilm. The concentration of these mediators is expected to increase by the growth of biofilm and the development of EPS which accumulates the mediators in the layers, limiting their diffusion into the environment.[16b] As observed in Figure 2D, this increases the current generated by *P. aeruginosa* in a condition where there is no direct contact with the surface. It is important noting that the planktonic (free-floating) and biofilm bacteria coexist and drive some exchanges between the two populations. The observed current, consequently, can be attributed to the collective contribution of both planktonic and biofilm bacteria, as they mutually share the EET mediators. However, the electron shuttles produced by planktonic bacteria might be oxidized by oxygen or easily lost through diffusion into the surrounding environment. Therefore, it is the biofilm bacteria that take on the major role in generating the current. Mechanism 2 refers to *S. aureus*, a Gram-positive bacterium with a thick cell wall composed of non-conducting peptidoglycan considered as a barrier to extracellular electron transfer. It has been, however, speculated that the bacteria might develop a weak current through the membrane-associated proteins[17] which remains constant during the biofilm formation possibly due to a competition between intracellular oxygen and the electrode surface as the terminal electron acceptor (Figure 2D). Mechanisms 3 and 4 describe the conditions in which *S. aureus* uses the redox mediators produced by *P. aeruginosa* either as the electron donor or as the electron acceptor. All these EET mechanisms collectively enhance the level of the generated current[16c,18] observed in Figure 2D. Mechanism 5 represents the possible way for mediator regeneration at the top layers of biofilm where the oxygen concentration is high. This pathway, however, is less possible in the middle and lower layers of biofilm due to the low diffusion and fast consumption of oxygen.[16b,19] In these layers, the electrode mainly operates as the terminal electron acceptor through the mechanisms explained above.

The current generated by the growth of biofilm in the bioanode drives the reduction of silver chloride to silver in the cathode layer

To demonstrate that the electrons released from a microbial biofilm can reduce the AgCl in the cathode layer, a simple design was proposed, as shown in Figure 3A. The setup comprised two parts, the cathode layer and the bioanode. The cathode is an AgCl layer bridging two silver legs of the inkjet printed electrode and the bioanode is a matured biofilm grown on carbon cloth in the co-culture of *S. aureus* and *P. aeruginosa.* Chronoamperometric measurements at an applied potential of 5 mV over the AgCl layer were conducted in LB medium. During the measurement, the biofilm containing bioanode has been connected to the inkjet printed electrode, practically, the bridge of AgCl layer. Figure 3B shows the results of the current measurement with calculated resistance of the AgCl/Ag transduction layer in the beginning (>40 M Ω; the layer dominated by AgCl) and the end (60 Ω; the layer dominated by Ag) of the experiment. For this particular electrode, after 75 s, a significant increase in current was observed. The striking increase in current from pA (approx. resistance of >40 MΩ) to 70 μA (approx. resistance of 60 Ω) confirms the conversion of AgCl to Ag by the current generated by the biofilm bioanode. The results prove that the described setup provides biofilm-to-resistance transduction, which we later exploit for wireless sensing of biofilm.

It is worth noting that the complete reduction of AgCl to Ag does not occur instantaneously. According to the data presented in Figure 3B, there is a sharp increase in current indicating the initial reduction of AgCl after 75 s. Subsequently, there is a gradual increase in current that levels off after 175 s. The process of reducing AgCl to metallic Ag begins at the Ag/AgCl interface, where Ag^+ ions, partially solvated within the solid AgCl film, support the ionic transport during the initial stages. As the reduction proceeds, Ag atoms are formed on the surface of the substrate (Ag/AgCl interface), with Ag^+ ions being supplied from the microchannels. In the next stages, the microchannel walls dissolve gradually, causing the channels to widen. These widened channels allow the electrolyte pene-

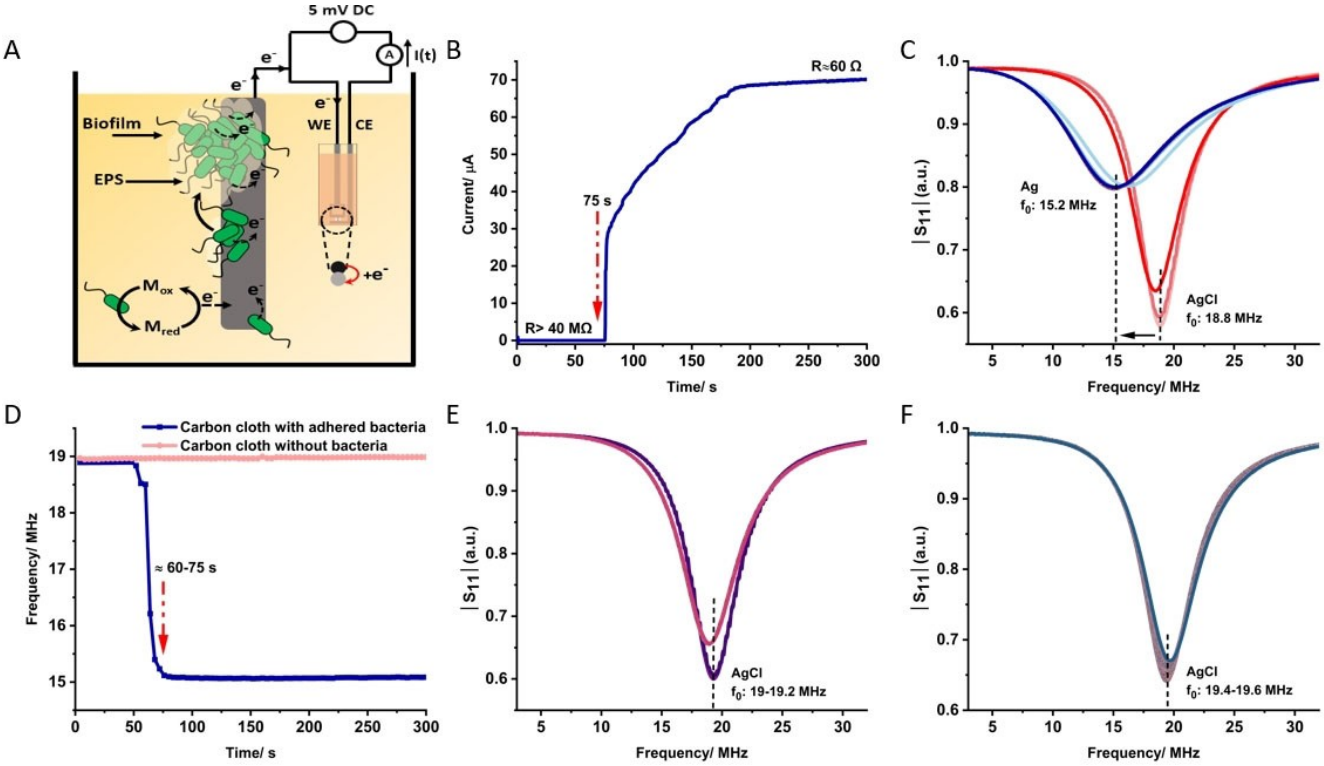

Figure 3. (A) Setup for amperometric measurements of the resistance of the cathode layer connected to the bioanode; both immersed in LB medium. The cathode layer comprised of AgCl, bridges two legs of IJPE. The IJPE is in connection with the carbon cloth bioanode with adhered biofilm. (B) Amperometric results, as obtained with the setup shown in (A). Time zero corresponds to the moment when the bioanode with mature biofilm has been connected to cathode. At 75 s, increased current indicates that the major part of AgCl in the cathode has been reduced to Ag by the current provided by the bioanode. (C) $|S_{11}|$ vs. frequency recorded in a setup sketched in Scheme 1. AgCl cathode layer hosting IJPE has been coupled as a part of tag antenna and connected to the carbon cloth with adhered, matured biofilm; both, the cathode and the bioanode have been immersed in LB medium. Time zero corresponds to the moment when the bioanode has been connected to the cathode. (D) Changes of the characteristic frequency of the wireless biosensor tag comprising of AgCl (cathode)/IJPE as a part of tag antenna in response to the cathode coupling to the carbon cloth bioanode with and without adhered, mature biofilm; both, cathode and bioanode are immersed in LB medium. (E) $|S_{11}|$ vs. frequency recorded for 12 h in a setup similar to scheme 1, in which AgCl/IJPE as a part of tag antenna is in connection with the bare carbon cloth (without any adhered planktonic bacteria or biofilm) immersed in sterile LB medium. (F) $|S_{11}|$ vs. frequency recorded for 12 h with a setup in which only AgCl/IJPE as a part of tag antenna is immersed in the co-culture of *S. aureus* and *P. aeruginosa* (10:1) dispersed in LB medium.

tration, leading to a transition in the primary charge carriers of the AgCl layer from partially solvated Ag^+ ions in the microchannels to fully solvated Cl^- ions in the widened channels which ultimately enables the complete reduction of AgCl to Ag.[20]

Proof-of-concept demonstration of wireless detection of matured microbial biofilm

In the experimental setup of this study a tag antenna enables a wireless signal sensing of the resistance (generally impedance) of the Ag-AgCl layer integrated into its coil. We exploit the property of antennas to reflect or absorb electromagnetic waves. Note that in case of absorption of electromagnetic wave, a current is generated in the antenna structure, i.e., an electromagnetic energy is absorbed (and dissipated) by the antenna. To monitor the absorption, a Vector Network Analyzer (VNA) is used. The VNA is equipped with its own antenna, which generates electromagnetic waves of different frequencies, thus, exposing the antenna of the sensor setup to electromagnetic field. For most of the frequencies the electromagnetic waves do not induce current in the sensor antenna, i.e., the antenna does not absorb electromagnetic energy. This case represents a complete reflection of the electromagnetic waves from the sensor antenna. At certain characteristic frequency (f_0) of the electromagnetic field, the sensor setup antenna will absorb the electromagnetic waves/energy. This wireless electromagnetic interaction between the two antennas is characterized by parameter $|S_{11}|$, known as the reflection coefficient (see also SI). The $|S_{11}|=1$ in case of full reflection and $|S_{11}|=0$ in case of full absorption. Practically, the $|S_{11}|$ is in between 0 and 1 and, obviously depends on frequency of electromagnetic field. Note that the frequency at which $|S_{11}|$ is at minimum is called the characteristic frequency.

To demonstrate the wireless sensing of a biofilm by the setup shown in Scheme 1, the inkjet printed electrode bridged by an AgCl layer (AgCl/IJPE) was connected to the RF (radio frequency) tag antenna. The electrode was immersed in LB medium and the $|S_{11}|$ characteristics of the antenna-electrode circuit were measured. As can be seen in Figure 3C, the AgCl/IJPE had a characteristic frequency of 18.8 MHz. After connecting the AgCl/IJPE to the biofilm grown on the carbon cloth bioanode, the characteristic frequency quickly shifted to 15.2 MHz, showing the reduction of AgCl layer to Ag by the current generated by the mature biofilm. The conversion of non-conductive AgCl to highly conductive Ag changed the impedance of the tag antenna, which thus acquired new characteristic frequency (f_0) and $|S_{11}|$ values. The plot of characteristic frequency vs. time in Figure 3D demonstrates that for this particular case, it takes 68 s ±7.5 to observe the change of the characteristic frequency and confirms the fast, wireless sensor response in detecting a matured biofilm capable to generate bioanode current in the range of 40–60 μA (Figure 2B). Compared to our previous studies on wireless detection of biological reactions, here, a close to minute short response time was obtained by exploiting inkjet printing for low volume deposition of Ag nanomaterials.

As the control and with the same setup, the $|S_{11}|$ characteristic was measured when AgCl/IJPE was connected to the bare carbon cloth (without any grown biofilm) in sterile LB medium. As can be seen in Figure 3E, the characteristic frequency did not show any shift proving that the conversion of AgCl to Ag (changes in frequency from high to low values) can only occur in the presence of bacteria. It is important to note that the slight changes in frequency observed in Figure 3E, are related to the changes of the overall impedance of the tag antenna when the second electrode (i.e., carbon cloth) is connected. Figure 3D also includes the plot of characteristic frequency vs. time for this control measurement, showing the constant frequency over time for bare carbon cloth compared to the one with adhered biofilm. Additional control measurements were performed in order to prove the role of the biofilm in the reduction of AgCl to Ag. For this purpose, only AgCl/IJPE was connected to the RF tag antenna and the magnitude of $|S_{11}|$ was recorded for 12 h in the co-culture of *S. aureus* and *P. aeruginosa.* As shown in Figure 3F, no frequency shift was observed for AgCl/IJPE (19.4–19.6 MHz). This confirms that the reduction process cannot happen directly on AgCl layer and there is a need for an external electrode (i.e., carbon cloth) which can host the growth of microorganisms.

Wireless detection of the growth of microbial biofilm in the early stages in standard growth medium and simulated wound fluid

To demonstrate the possibility of early detection of biofilm formation using the proposed wireless system, AgCl/IJPE and carbon cloth were connected to the RF tag antenna according to the setup shown in Scheme 1 and their $|S_{11}|$ characteristic was measured in the co-culture of *S. aureus* and *P. aeruginosa.* The AgCl/IJPE-carbon cloth antenna coupled circuit showed an initial characteristic frequency of 18.0 MHz, Figure 4A. At the start, the frequency is constant but starts to shift toward lower frequencies after 21 min ± 1.5, and eventually settles at the characteristic frequency of 14.8 MHz (Figure 4B). In principle, when bacteria make contact with the carbon cloth, cell attachment occurs in two successive steps, the first of which is reversible and the second irreversible, which is known as the early stages of biofilm formation. In this stage, the carbon cloth can be used as the sink of electrons by *S. aureus* and *P. aeruginosa* by the mechanism of EET. The transferred electrons or the current generated by bacteria will be then consumed to reduce AgCl to Ag on AgCl/IJPE. The time taken for this conversion depends on the level of generated current and the amount of AgCl deposited on the cathode layer. As shown in Figure 4B, for this case, with the initial bacterial concentration of 10^6:10^5 CFU/mL (S. *aureus*: *P. aeruginosa*), it took 21 min ± 1.5 to reduce AgCl to Ag on AgCl/IJPE. Such a rapid response of the sensor system indicates its ability to detect the presence of bacteria in the early stages of biofilm formation. Concluding, it should be emphasized

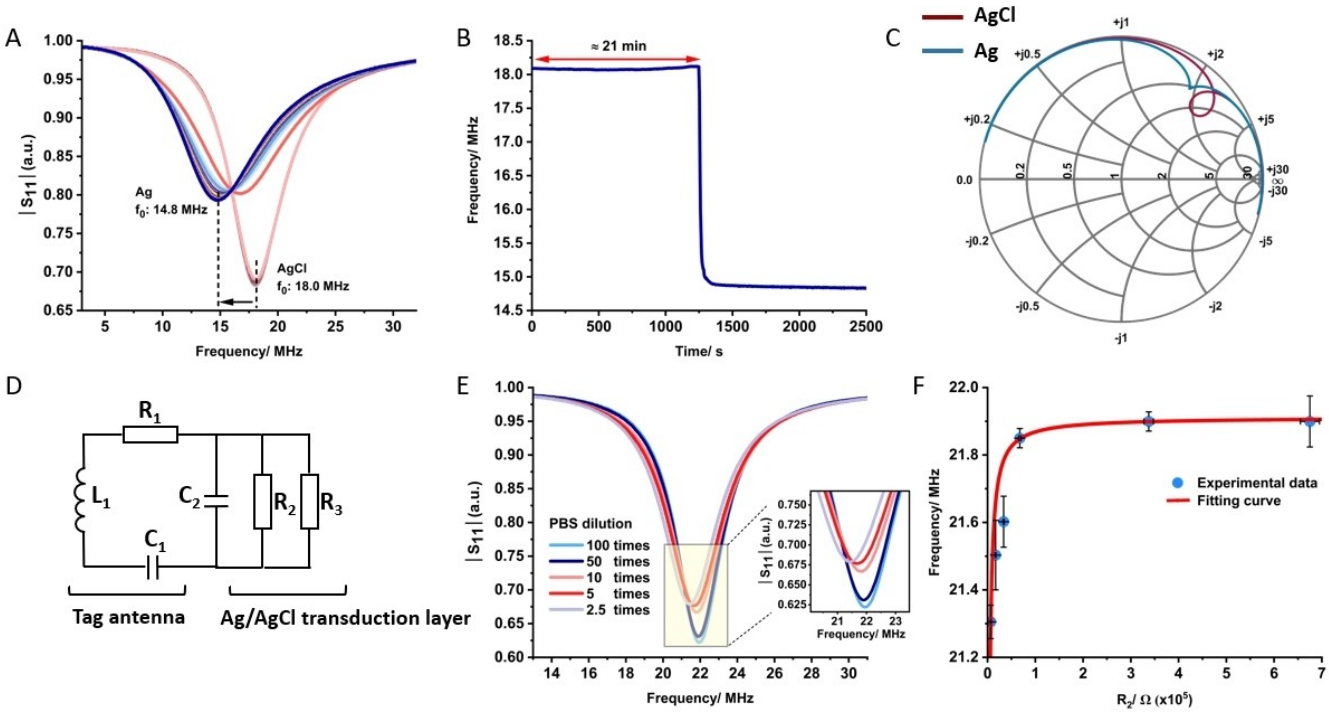

Figure 4. (A) $|S_{11}|$ vs. frequency recorded in a setup similar to scheme 1, in which AgCl/IJPE as a part of tag antenna is in connection with the carbon cloth and both are immersed in the co-culture of *S. aureus* and *P. aeruginosa* (10:1) dispersed in LB medium. (B) Changes of the characteristic frequency of the wireless biosensor comprised of AgCl/IJPE as a part of the tag antenna connected to the carbon cloth in response to the presence of the co-culture of *S. aureus* and *P. aeruginosa* (10:1) dispersed in LB medium. (C) Smith chart visualizing the complex impedance as AgCl converts to Ag. The measurements were performed with AgCl/IJPE as a part of the tag antenna in connection with the carbon cloth both immersed in the co-culture of *S. aureus* and *P. aeruginosa* (10:1) dispersed in LB medium. (D) Proposed equivalent circuit of the RF tag antenna integrated with the Ag/AgCl transduction layer. (E) The ionic strength dependencies of $|S_{11}|$ and the characteristic frequency f_0 measured for AgCl/IJPE. (F) Fitting of the experimental data describing the dependency of the characteristic frequency on the resistance of the solution (R_2) for AgCl/IJPE. The red curve shows the fit and the blue points represent the experimental data.

that the reproducible deposition of small amount of nanomaterials enabled by inkjet printing was found to be essential to demonstrate early stage biofilm detection. More discussions about the response time in relation to the generated current and characteristics of the cathode layer (AgCl/IJPE) are provided in Supporting Information, Sections S5 and S6.

To investigate the functionality of the proposed wireless setup in the early detection of microbial biofilm grown in close to authentic clinical setting, the measurements of the characteristic frequency were performed in simulated wound fluid, SWF. The AgCl/IJPE and carbon cloth were connected to the RF tag antenna and were placed in simulated wound fluid containing the co-culture of *S. aureus* and *P. aeruginosa.* The results of the characteristic frequency measurements provided in Figures S6A, and S6B show the conversion of AgCl to Ag occurring in $4\,\text{min} \pm 1.5$. The shorter response time observed in SWF compared to the LB medium could be related to the presence of human serum proteins; in fact, adhesion of *S. aureus* and *P. aeruginosa* to the surface can be promoted through binding bacterial cells to the serum proteins.[21] The control experiment in sterile SWF (with no adhered planktonic bacteria or biofilm on the carbon cloth) showed no frequency shift from the registered values for AgCl/IJPE (20.5 MHz) (Figure S6B and S6 C). This confirms that the human serum components including urea, creatinine, uric acid, and proteins do not transfer electrons to the carbon cloth sufficient to reduce AgCl to Ag in the cathode layer. Thus, in SWF, bacteria are the only electroactive species which carry out the conversion of AgCl to Ag.

Description of the equivalent electrical circuit of the chip-less, wireless biosensor

The proposed wireless setup for detecting bacteria is comprised of a bioanode part and the cathode layer. The cathode integrates Ag/AgCl redox conversion in the circuit of the radio frequency, RF, tag antenna. The changes of the cathode resistance, caused by the presence of bacteria on the bioanode, enable wireless biofilm sensing. Figure 4C shows the Smith chart visualizing the complex impedance as a function of frequency for the initial and final result of $|S_{11}|$ measurement shown in Figure 4A. Upon conversion of AgCl to Ag, the circuit exhibits a change in input impedance at the characteristic frequency from $Z_{in} = 1.555 + 2.002\text{j}$ to $Z_{in} = 0.553 + 1.885\text{j}$. This reveals significant alterations in the real part of the impedance (resistance) compared to the imaginary part (inductance).

Accounting the dominant resistive change of the tag antenna during the biofilm detection, we proposed the equivalent circuit shown in Figure 4D. The circuit is comprised of the RF tag antenna integrated with the Ag/AgCl transduction layer, where R_1, L_1 and C_1 represent the resistance, inductance, and capacitance of the tag antenna. C_2 is the parasitic capacitance of the antenna-IJPE connections. R_2 represents the resistance of the solution (dominates when the transduction layer is AgCl) and R_3 is the resistance of Ag/AgCl transduction layer. To confirm the validity of the proposed equivalent circuit, the $|S_{11}|$ and the characteristic frequency f_0 were measured for both Ag and AgCl/IJPE immersed in air, water, and buffer solutions of different ionic strength. As can be seen in Table S2, compared to Ag/IJPE, the characteristic frequency f_0 is dependent on the dilution of buffer solutions when the transduction layer is made of AgCl. The ionic strength dependencies of $|S_{11}|$ and the characteristic frequency f_0 measured for AgCl/IJPE are presented in Figure 4E. The characteristic frequency and attenuations shift to lower values at increasing ionic strength of the solution, possibly due to the increase in ionic conductivity of the AgCl layer. Figure 4F and (Figure S6D) show a similar dependency of characteristic frequency vs. R_2 values. As mentioned above, R_2 is the resistance of the solution and will be decreased by increasing the ionic strength. R_2 values can be extracted from electrochemical impedance spectroscopy data measured for AgCl/IJPE immersed in buffer solutions with different ionic strength (data shown in Table S2). The experimental data presented in the plot of the characteristic frequency vs. R_2 (Figure 4F) were then modeled using the procedure described in the next paragraph.

The proposed equivalent circuit of the biosensor tag shown in Figure 4D was used to derive the equations 1–3 for fitting of the dependency of frequency on the resistance of the solution (R_2) as shown in Figure 4F:

$$Z_{Re} = \frac{(R_2 + R_3)R_2 R_3}{C_2^2\omega^2 R_2^2 R_3^2 + (R_2 + R_3)^2} + R_1 \quad (1)$$

$$Z_{Im} = L_1\omega - \frac{1}{C_1\omega} - \frac{C_2\omega R_2^2 R_3^2}{C_2^2\omega^2 R_2^2 R_3^2 + (R_2 + R_3)^2} \quad (2)$$

Where $\omega = 2\pi f$. Considering the condition for the characteristic frequency, $\omega_0 = 2\pi f_0$, $Z_{Im} = 0$, the following equation will be obtained:

$$f_0^2 = \left(2\pi^2 \left(\begin{array}{c} \sqrt{\frac{4C_1C_2^2L_1R_2^2R_3^2}{(R_2+R_3)^2} + \left(C_1L_1 - \frac{C_2R_2^2R_3^2\ (C_1+C_2)}{(R_2+R_3)^2}\right)^2} \\ -\frac{C_1C_2R_2^2R_3^2}{(R_2+R_3)^2} + C_1L_1 - \frac{C_2^2R_2^2R_3^2}{(R_2+R_3)^2} \end{array} \right) \right)^{-1} \quad (3)$$

The equations were written in Mathematica symbolic language and fitted to experimental values of frequency. As can be seen in Figure 4F, the fitting curve (shown by a line) describes well the experimental data of dependency of frequency on solution resistance (shown by points). The fitting was then used to extract the corresponding values of the circuit elements of R_1, L_1, C_1, and C_2 as 19.3 Ω ± 1.3, 10900 pH ± 300, 53 nF ± 3, and 27 pF ± 4, respectively. The good agreement between the fitting and experimental data confirms that the proposed equivalent circuit can be used for describing the RF tag antenna circuit with integrated Ag/AgCl transduction layer. Based on this modeling, the Ag/AgCl transduction layer and the adjacent PBS solution can be represented by resistors (R_2 and R_3) inserted as a part of the tag antenna which relates the Ag/AgCl redox conversion to the electron transfer reaction of microorganisms for wireless sensing of bacteria.

Conclusion

In this work, we have introduced a new, rapidly responsive sensor design for wireless detection of microbial biofilms. The design comprised of electrically conducting material, specifically carbon cloth, which acted as a biofilm hosting bioanode. A layer of AgCl, integrated as a part of tag antenna coil, acted as a transducing cathode. In this setup bacterial biofilms on the bioanode electroreduced AgCl to Ag. The AgCl to Ag redox transition strongly changed the impedance of the tag antenna, which was wirelessly detected by recording the reflection coefficient of the antenna, $|S_{11}|$, and the characteristic frequency of the tag. The wireless biofilm sensing was demonstrated for biofilm formed by medically relevant co-culture, comprised of *S. aureus* and *P. aeruginosa* in concentration ratio 10^6:10^5 CFU/mL, respectively.

The biofilm formation by the bacteria was confirmed by scanning electron and confocal microscopies. Extracellular electron transfer from the biofilm to the carbon cloth was proven by measurements of the biofilm generated current and recordings of open circuit potential. One of the fundamentally important results of this study is the demonstration that co-cultures of these bacteria form biofilms, generate higher bioanode currents than biofilms of their monocultures. The synergism in extracellular electron transfer indicates that detection of multi-specie infections, and especially of infections leading to chronic wounds, with the presence of strong electrogene such as *P. aeruginosa*, might be easier in clinical setting.

A few of the most important results of this study can be summarized as follows. We demonstrate that the presented wireless sensor design allows detection of mature biofilms in minutes. This was proven by coupling bioanode hosting mature biofilm to the antenna integrated AgCl cathode. In our specific experimental setup, the mature biofilm detection was realized in 68 s ± 7.5. To demonstrate a possibility for early-stage biofilm detection, the inkjet-printed cathode and the bioanode comprised of bacteria-free carbon cloth were immersed into the *S. aureus* and *P. aeruginosa* co-culture. It took 21 min ± 1.5 for wireless sensor system to report the presence of the bacteria in the LB cell culture. When simulated wound fluid was used instead of the LB medium, the system responded to the presence of bacteria co-culture in 4 min ± 1.5. Such a rapid response we assigned to facile bacteria adhesion to the carbon cloth and wireless detection of biofilms in their earliest stages of formation.

This breakthrough has been possible only due to reproducible, low amount of deposition of nanomaterials offered by inkjet printing technology. Specifically, deposition of low amounts of Ag nanoparticles and then electrochemical conversion of the Ag layer to make an AgCl transducing cathode integrated into the tag antenna coil was essential. The requirement of high-end deposition and stabilization of transducing cathode layer by inkjet printing might be considered as limitation in broad replication of the proposed setup. However, the demonstration of rapid detection of bacterial attachment to surfaces and detection of early-stage biofilms are encouraging for future development and application of this wireless sensors setup for detection of wound infections.

Some consideration can be noted regarding the formal potential of the Ag/AgCl redox couple ($E^{0'} = +0.2$ V) which lies in the middle of the reduction potentials for biologically relevant reactions. The proposed configuration represents a universal setup, which could be also recommended for wireless tracking of cathodic biofilms. These biofilms should have the capacity to drive the oxidation of Ag to AgCl. One example is the nitrate-reducing bacteria, which possess the enzyme nitrate reductase enabling the reduction of nitrate into nitrite ($E^{0'} = +0.42$ V) or other nitrogenous compounds.[22] In the absence of oxygen ($E^{0'} = 0.82$ V), these bacteria utilize nitrate as the terminal electron acceptor in the biocathode, with the electrons being supplied from the Ag to AgCl conversion taking place in the anode.

Acknowledgements

We acknowledge the Swedish Research Council (2018-04320), the Knowledge Foundation (20170058 and 20190010), and Mats Paulsson's foundation for Research, Innovation and Development of Society for financial support. We especially thank Julia Davies and Madeleine Blomqvist at the Department of Oral Biology, Faculty of Odontology, Malmö University for help with confocal laser scanning microscopy.

Conflict of Interest

The authors declare no conflict of interest.

Data Availability Statement

The data that support the findings of this study are available from the corresponding author upon reasonable request.

Keywords: Chip-Less Wireless Sensing · Inkjet Printing · Mediated Electron Transfer · Microbial Biofilm · Near Field Communication

[1] a) N. Høiby, T. Bjarnsholt, M. Givskov, S. Molin, O. Ciofu, *Int. J. Antimicrob. Agents* **2010**, *35*, 322–332; b) T. Bjarnsholt, *APMIS* **2013**, *121*, 1–58; c) T. Bjarnsholt, K. Kirketerp-Møller, P. Ø. Jensen, K. G. Madsen, R. Phipps, K. Krogfelt, N. Høiby, M. Givskov, *Wound Rep. Reg.* **2008**, *16*, 2–10; d) N. Høiby, O. Ciofu, H. K. Johansen, Z. j. Song, C. Moser, P. Ø. Jensen, S. Molin, M. Givskov, T. Tolker-Nielsen, T. Bjarnsholt, *Int. J. Oral Sci.* **2011**, *3*, 55–65.

[2] a) I. Barros Almeida, L. Garcez Barretto Teixeira, F. Oliveira de Carvalho, É. Ramos Silva, P. Santos Nunes, M. R. Viana dos Santos, A. Antunes de Souza Araújo, *Adv. Skin Wound Care* **2021**, *34*, 1–8; b) Q. Pang, D. Lou, S. Li, G. Wang, B. Qiao, S. Dong, L. Ma, C. Gao, Z. Wu, *Adv. Sci.* **2020**, *7*, 1902673; c) S. L. Percival, K. E. Hill, D. W. Williams, S. J. Hooper, D. W. Thomas, J. W. Costerton, *Wound Rep. Reg.* **2012**, *20*, 647–657.

[3] a) R. Jarošová, S. E. McClure, M. Gajda, M. Jović, H. H. Girault, A. Lesch, M. Maiden, C. Waters, G. M. Swain, *Anal. Chem.* **2019**, *91*, 8835–8844; b) N. T. Thet, D. R. Alves, J. E. Bean, S. Booth, J. Nzakizwanayo, A. E. R. Young, B. V. Jones, A. T. A. Jenkins, *ACS Appl. Mater. Interfaces* **2016**, *8*, 14909–14919; c) N. T. Thet, J. Mercer-Chalmers, R. J. Greenwood, A. E. R. Young, K. Coy, S. Booth, A. Sack, A. T. A. Jenkins, *ACS Sens.* **2020**, *5*, 2652–2657.

[4] a) M. Magana, C. Sereti, A. Ioannidis, C. A. Mitchell, A. R. Ball, E. Magiorkinis, S. Chatzipanagiotou, M. R. Hamblin, M. Hadjifrangiskou, G. P. Tegos, *Clin. Microbiol. Rev.* **2018**, *31*; b) N. B. S. Silva, L. A. Marques, D. D. B. Röder, *J. Appl. Microbiol.* **2021**, *131*, 2148–2160; c) R. Funari, A. Q. Shen, *ACS Sens.* **2022**, *7*, 347–357; d) T. F. Bahamondez-Canas, L. A. Heersema, H. D. C. Smyth, *Biomedicine* **2019**, *7*, 34.

[5] B. Farahani, F. Firouzi, V. Chang, M. Badaroglu, N. Constant, K. Mankodiya, *Future Gener. Comput. Syst.* **2018**, *78*, 659–676.

[6] a) P. Escobedo, M. Bhattacharjee, F. Nikbakhtnasrabadi, R. Dahiya, *IEEE Internet Things J.* **2021**, *8*, 5093–5100; b) M. F. Farooqui, A. Shamim, *Sci. Rep.* **2016**, *6*, 28949.

[7] a) S. Darvishi, S. Tavakoli, M. Kharaziha, H. H. Girault, C. F. Kaminski, I. Mela, *Angew. Chem. Int. Ed.* **2022**, *61*, e202112218; b) S. RoyChoudhury, Y. Umasankar, J. Jaller, I. Herskovitz, J. Mervis, E. Darwin, P. A. Hirt, L. J. Borda, H. A. Lev-Tov, R. Kirsner, S. Bhansali, *J. Electrochem. Soc.* **2018**, *165*, B3168-B3175; c) Z. Xiong, S. Achavananthadith, S. Lian, L. E. Madden, Z. X. Ong, W. Chua, V. Kalidasan, Z. Li, Z. Liu, P. Singh, *Sci. Adv.* **2021**, *7*, eabj1617.

[8] a) C. Santoro, C. Arbizzani, B. Erable, I. Ieropoulos, *J. Power Sources* **2017**, *356*, 225–244; b) H. Yang, M. Zhou, M. Liu, W. Yang, T. Gu, *Biotechnol. Lett.* **2015**, *37*, 2357–2364; c) O. Obata, M. J. Salar-Garcia, J. Greenman, H. Kurt, K. Chandran, I. Ieropoulos, *J. Environ. Manage.* **2020**, *258*, 109992; d) J. Greenman, I. Gajda, J. You, B. A. Mendis, O. Obata, G. Pasternak, I. Ieropoulos, *Biofilm* **2021**, *3*, 100057; e) M. N. Gatti, R. H. Milocco, *Int. J. Energy Environ. Eng.* **2017**, *8*, 303–315.

[9] a) R. C. Huiszoon, S. Subramanian, P. R. Rajasekaran, L. A. Beardslee, W. E. Bentley, R. Ghodssi, *IEEE Trans. Biomed. Eng.* **2018**, *66*, 1337–1345; b) P. Pang, X. Xiao, Q. Cai, S. Yao, C. A. Grimes, *Sens. Actuators B* **2008**, *133*, 473–477; c) H. Wang, A. J. F. Tampio, Y. Xu, B. D. Nicholas, D. Ren, *ACS Biomater. Sci. Eng.* **2020**, *6*, 727–738.

[10] a) M. Forouzandeh, N. C. Karmakar, *Wireless Power Transfer* **2015**, *2*, 62–77; b) C. Herrojo, F. Paredes, J. Mata-Contreras, F. Martín, *Sensors* **2019**, *19*, 3385; c) P. Kalimuthu, J. F. Gonzalez-Martinez, D. Jakubauskas, M. Cárdenas, T. Ruzgas, J. Sotres, *Electrochim. Acta* **2021**, *381*, 138275; d) P. Kalimuthu, J. F. Gonzalez-Martinez, T. Ruzgas, J. Sotres, *Anal. Chem.* **2020**, *92*, 13110–13117; e) T. Ruzgas, N. Larpant, A. Shafaat, J. Sotres, *ChemElectroChem* **2019**, *6*, 5167–5171.

[11] a) N. Larpant, A. D. Pham, A. Shafaat, J. F. Gonzalez-Martinez, J. Sotres, J. Sjöholm, W. Laiwattanapaisal, F.

Faridbod, M. R. Ganjali, T. Arnebrant, T. Ruzgas, *Sci. Rep.* **2019**, *9*, 12948; b) V. C. Hoang, A. Shafaat, S. Jankovskaja, V. G. Gomes, T. Ruzgas, *Biosens. Bioelectron.* **2021**, *191*, 113420.

[12] A. Shafaat, R. Žalnėravičius, D. Ratautas, M. Dagys, R. Meškys, R. Rutkienė, J. F. Gonzalez-Martinez, J. Neilands, S. Björklund, J. Sotres, T. Ruzgas, *ACS Sens.* **2022**, *7*, 1222–1234.

[13] a) W. O. Silva, V. Costa Bassetto, D. Baster, M. Mensi, E. Oveisi, H. H. Girault, *ACS Appl. Electron. Mater.* **2020**, *2*, 927–935; b) V. Costa Bassetto, M. Mensi, E. Oveisi, H. H. Girault, A. Lesch, *ACS Appl. Energ. Mater.* **2019**, *2*, 6322–6331; c) A. Lesch, *Adv. Mater. Technol.* **2018**, *3*, 1700201; d) M. Jović, Y. Zhu, A. Lesch, A. Bondarenko, F. Cortés-Salazar, F. Gumy, H. H. Girault, *J. Electroanal. Chem.* **2017**, *786*, 69–76; e) A. Lesch, F. Cortés-Salazar, V. Amstutz, P. Tacchini, H. H. Girault, *Anal. Chem.* **2015**, *87*, 1026–1033.

[14] a) C. B. Ibberson, A. Stacy, D. Fleming, J. L. Dees, K. Rumbaugh, M. S. Gilmore, M. Whiteley, *Nat. Microbiol.* **2017**, *2*, 17079; b) A. R. Siddiqui, J. M. Bernstein, *Clin. Dermatol.* **2010**, *28*, 519–526; c) B. A. R. N. Durand, C. Pouget, C. Magnan, V. Molle, J.-P. Lavigne, C. Dunyach-Remy, *Microorganisms* **2022**, *10*, 1500.

[15] a) C. Berne, C. K. Ellison, A. Ducret, Y. V. Brun, *Nat. Rev. Microbiol.* **2018**, *16*, 616–627; b) H. H. Tuson, D. B. Weibel, *Soft Matter* **2013**, *9*, 4368–4380; c) T. E. P. Kimkes, M. Heinemann, *FEMS Microbiol. Rev.* **2020**, *44*, 106–122.

[16] a) F. Kracke, I. Vassilev, J. O. Krömer, *Front. Microbiol.* **2015**, *6*; b) M. E. Hernandez, D. K. Newman, *Cell. Mol. Life Sci.* **2001**, *58*, 1562–1571; c) T. H. Pham, N. Boon, K. De Maeyer, M. Höfte, K. Rabaey, W. Verstraete, *Appl. Microbiol. Biotechnol.* **2008**, *80*, 985–993; d) Y. Yang, M. Xu, J. Guo, G. Sun, *Process Biochem.* **2012**, *47*, 1707–1714; e) K. Rabaey, N. Boon, M. Höfte, W. Verstraete, *Environ. Sci. Technol.* **2005**, *39*, 3401–3408; f) Y. Wang, D. K. Newman, *Environ. Sci. Technol.* **2008**, *42*, 2380–2386.

[17] a) G. Pankratova, L. Hederstedt, L. Gorton, *Anal. Chim. Acta* **2019**, *1076*, 32–47; b) R. Y. A. Hassan, U. Wollenberger, *Anal. Bioanal. Chem.* **2016**, *408*, 579–587; c) G. Wang, H. Feng, A. Gao, Q. Hao, W. Jin, X. Peng, W. Li, G. Wu, P. K. Chu, *ACS Appl. Mater. Interfaces* **2016**, *8*, 24509–24516; d) J. Zhao, F. Li, Y. Cao, X. Zhang, T. Chen, H. Song, Z. Wang, *Biotechnol. Adv.* **2021**, *53*, 107682; e) X. Xiao, H.-Q. Yu, *Curr. Opin. Chem. Biol.* **2020**, *59*, 104–110.

[18] E. M. Bosire, L. M. Blank, M. A. Rosenbaum, *Appl. Environ. Microbiol.* **2016**, *82*, 5026–5038.

[19] a) Y. Tokunou, M. Toyofuku, N. Nomura, *mBio* **2022**, *13*, e01957–01922; b) S. H. Saunders, E. C. M. Tse, M. D. Yates, F. J. Otero, S. A. Trammell, E. D. A. Stemp, J. K. Barton, L. M. Tender, D. K. Newman, *Cell* **2020**, *182*, 919–932.e919.

[20] a) X. Jin, J. Lu, P. Liu, H. Tong, *J. Electroanal. Chem.* **2003**, *542*, 85–96; b) T. Katan, S. Szpak, D. N. Bennion, *J. Electrochem. Soc.* **1974**, *121*, 757; c) V. I. Birss, C. K. Smith, *Electrochim. Acta* **1987**, *32*, 259–268; d) G. W. D. Briggs, H. R. Thirsk, *Trans. Faraday Soc.* **1952**, *48*, 1171–1178.

[21] a) M. Pihl, A. Arvidsson, M. Skepö, M. Nilsson, M. Givskov, T. Tolker-Nielsen, G. Svensäter, J. R. Davies, *Pathog. Dis.* **2013**, *67*, 192–198; b) A. P. Cardile, C. J. Sanchez, M. E. Samberg, D. R. Romano, S. K. Hardy, J. C. Wenke, C. K. Murray, K. S. Akers, *BMC Res. Notes* **2014**, *7*, 457; c) C. García-Bonillo, R. Texidó, G. Reyes-Carmenaty, J. Gilabert-Porres, S. Borrós, *ACS Appl. Bio Mater.* **2020**, *3*, 3354–3364.

[22] a) M. Rosenbaum, F. Aulenta, M. Villano, L. T. Angenent, *Bioresour. Technol.* **2011**, *102*, 324–333; b) P. Clauwaert, K. Rabaey, P. Aelterman, L. De Schamphelaire, T. H. Pham, P. Boeckx, N. Boon, W. Verstraete, *Environ. Sci. Technol.* **2007**, *41*, 3354–3360; c) M. Tiso, A. N. Schechter, *PLoS One* **2015**, *10*, e0119712; d) A. Bhusal, P. M. Muriana, *Appl. Microbiol.* **2021**, *1*, 11–23.

Manuscript received: June 10, 2023
Accepted manuscript online: July 25, 2023
Version of record online: August 25, 2023